



**Providing Choice & Value**

Generic CT and MRI Contrast Agents



**FRESENIUS  
KABI**

**CONTACT REP**

**AJNR**

This information is current as  
of July 22, 2025.

## **Correlation between Multiparametric MR Imaging and Molecular Genetics in Pontine Pediatric High-Grade Glioma**












V. Rameh, S. Vajapeyam, A. Ziaei, P. Kao, W.B. London,  
S.J. Baker, J. Chiang, J. Lucas, C.L. Tinkle, K.D. Wright and  
T.Y. Poussaint

*AJNR Am J Neuroradiol* 2023, 44 (7) 833-840

doi: <https://doi.org/10.3174/ajnr.A7910>

<http://www.ajnr.org/content/44/7/833>

# Correlation between Multiparametric MR Imaging and Molecular Genetics in Pontine Pediatric High-Grade Glioma

 V. Rameh,  S. Vajapeyam,  A. Ziaei,  P. Kao,  W.B. London,  S.J. Baker,  J. Chiang,  J. Lucas,  C.L. Tinkle,  K.D. Wright, and  T.Y. Poussaint



## ABSTRACT

**BACKGROUND AND PURPOSE:** Molecular profiling is a crucial feature in the “integrated diagnosis” of CNS tumors. We aimed to determine whether radiomics could distinguish molecular types of pontine pediatric high-grade gliomas that have similar/overlapping phenotypes on conventional anatomic MR images.

**MATERIALS AND METHODS:** Baseline MR images from children with pontine pediatric high-grade gliomas were analyzed. Retrospective imaging studies included standard precontrast and postcontrast sequences and DTI. Imaging analyses included median, mean, mode, skewness, and kurtosis of the ADC histogram of the tumor volume based on T2 FLAIR and enhancement at baseline. Histone H3 mutations were identified through immunohistochemistry and/or Sanger or next-generation DNA sequencing. The log-rank test identified imaging factors prognostic of survival from the time of diagnosis. Wilcoxon rank-sum and Fisher exact tests compared imaging predictors among groups.

**RESULTS:** Eighty-three patients had pretreatment MR imaging and evaluable tissue sampling. The median age was 6 years (range, 0.7–17 years); 50 tumors had a K27M mutation in *H3-3A*, and 11, in *H3C2/3*. Seven tumors had histone H3 K27 alteration, but the specific gene was unknown. Fifteen were H3 wild-type. Overall survival was significantly higher in *H3C2/3*- compared with *H3-3A*-mutant tumors ( $P = .003$ ) and in wild-type tumors compared with any histone mutation ( $P = .001$ ). Lower overall survival was observed in patients with enhancing tumors ( $P = .02$ ) compared with those without enhancement. *H3C2/3*-mutant tumors showed higher mean, median, and mode ADC<sub>total</sub> values ( $P < .001$ ) and ADC<sub>enhancement</sub> ( $P < .004$ ), with lower ADC<sub>total</sub> skewness and kurtosis ( $P < .003$ ) relative to *H3-3A*-mutant tumors.

**CONCLUSIONS:** ADC histogram parameters are correlated with histone H3 mutation status in pontine pediatric high-grade glioma.

**ABBREVIATIONS:** DIPG = diffuse intrinsic pontine glioma; DMG = diffuse midline glioma; HGG = high-grade glioma; IDH = isocitrate dehydrogenase; OS = overall survival; PG = postgadolinium; pHGG = pediatric-type high-grade glioma

**D**iffuse intrinsic pontine glioma (DIPG) is defined as an expansile T1-hypointense, T2-hyperintense nonenhancing pontine tumor involving at least 50% of the ventral pons and engulfing the basilar artery.<sup>1–3</sup> These tumors were reclassified in

the 2021 World Health Organization classification of CNS tumors, emphasizing that molecular features are as essential as histology in diagnosing pontine tumors.<sup>3,4</sup> Numerous molecular changes of clinicopathologic utility were incorporated, and the designation of a subset of tumors formerly called DIPG as H3 K27–altered diffuse midline glioma highlights the importance of this mutation in defining a disease entity.<sup>2,3</sup>

Pontine H3 K27–altered diffuse midline glioma (DMG) is an aggressive pediatric-type high-grade glioma (pHGG) with a median age at diagnosis of 6–7 years and a poor prognosis, with <10% overall survival (OS) of >2 years.<sup>5–7</sup> The diagnosis has historically been based on clinical and MR imaging characteristics.<sup>1</sup> Surgery was not considered an option due to the location and infiltrative nature of the tumor, and biopsy was uncommonly performed after weighing risks and benefits.<sup>8</sup>


Recently, feasible and safe biopsies and postmortem examinations have led to a greater understanding of the unique genetic profiles of these tumors and the consequent identification of new

Received March 9, 2023; accepted after revision May 22.

From the Department of Radiology (V.R., S.V., A.Z., T.Y.P.), Boston Children's Hospital, Harvard Medical School, Boston, Massachusetts; Department of Pediatric Oncology (P.K., W.B.L., K.D.W.), Dana-Farber Cancer Institute, Harvard Medical School, Boston, Massachusetts; and Departments of Developmental Neurobiology (S.J.B.), Pathology (J.C.), and Radiation Oncology (J.L., C.L.T.), St. Jude Children's Research Hospital, Memphis, Tennessee.

This work was supported, in part, by the American Lebanese Syrian Associated Charities and the National Cancer Institute grant P30 CA021765 (St. Jude Cancer Center support grant) and P01 CA096832.

Please address correspondence to Tina Young Poussaint, MD, Department of Radiology, Boston Children's Hospital, 300 Longwood Ave, Boston, MA 02115; e-mail: tinayoung.poussaint@childrens.harvard.edu; @TYPoussaintMD; @vanessaramel

 Indicates open access to non-subscribers at [www.ajnr.org](http://www.ajnr.org)

 Indicates article with online supplemental data.

<http://dx.doi.org/10.3174/ajnr.A7910>

potential therapeutic targets.<sup>9-11</sup> Specifically, the somatic mutations of histone H3 genes (*H3-3A* and *H3C2/3*), leading to their protein products H3.3 and H3.1, respectively, and the substitution of a lysine for methionine have been identified. Up to 90% of pontine high-grade gliomas (HGGs) have an H3 mutation, with ~65% in *H3-3A* and ~25% in *H3C2/3*. Approximately 10% of pontine HGGs lack an H3 mutation.<sup>5,10,12-14</sup> Advances in “liquid biopsy,” namely the ability to detect these mutations in circulating tumor DNA or CSF tumor DNA, may enable noninvasive testing of molecular profiling in DMG and longitudinal monitoring when the patient is on therapy.<sup>15,16</sup>

Prior investigators identified certain MR imaging features associated with worse prognosis in pontine HGGs, such as shorter survival in patients with lower mean ADC histogram values, a lower Cho/Cr ratio on MRS, and the presence of the H3 K27 alteration.<sup>17-19</sup>

It is now increasingly understood that different genomic alterations in histone H3 isoforms result in tumors with variable behavior and clinical prognosis, including differences between *H3C2/3*- and *H3-3A*-mutant tumors.<sup>20-22</sup>

To date, few studies have elucidated these differences using radiogenomic methods. This emerging technique uses primarily pretreatment baseline multiparametric MR imaging features and correlates them with pathologic and molecular data obtained from a specific tissue biopsy site.<sup>12,18,23-26</sup> Furthermore, a more recently described, multimodel approach proposed the use of MR imaging radiomics and clinical data to predict at least 1 of 3 important mutations (*H3.1*, *ACVR1*, and *TP53*) in pontine pHGGs. This efficient model can be used with the absence of data on biopsy and/or genetic results.<sup>27</sup>

In this study, we correlated different baseline MR imaging features and OS in pontine pHGG subtypes with molecular parameters using ADC histogram analyses in a large cohort of children newly diagnosed with pontine HGG who underwent tissue sampling.

## MATERIALS AND METHODS

### Subjects

This was a retrospective study approved by the institutional review board and performed in accordance with the Declaration of Helsinki. All consecutive patients who were clinically diagnosed with DIPG or pontine DMG at the time of presentation at St. Jude Children’s Research Hospital between 2002 and 2019 and had postmortem or biopsy data and baseline MR images were included. Each patient underwent histologic tumor evaluation at postmortem examination following unsuccessful therapy and/or stereotactic biopsy before initiation of treatment, with the choice of biopsy site left to the neurosurgeon’s discretion.

Immunohistochemistry or next-generation DNA sequencing or both were used to identify histone H3 mutations, as previously described.<sup>28</sup> We defined 4 H3 mutation groups: 1) *H3-3A* K27-mutant; 2) *H3C2-/H3C3* K27-mutant; 3) H3 K27-mutant, specific genes were unknown; and 4) H3 wild-type. The latter may include pHGG (DMG, H3 K27-altered, subtype H3 wild-type with *EZH1* overexpression, and pHGG, H3 wild-type and isocitrate dehydrogenase [*IDH*] wild-type) or adult-type diffuse glioma (astrocytoma, *IDH* mutant and glioblastoma, *IDH* wild-type).<sup>3</sup> Overall survival was measured for all patients, calculated as the length of time from diagnosis to death and/or the last follow-up.

### Imaging Analysis

Baseline MR imaging of the brain was used for analysis as previously described.<sup>24</sup> MR imaging examinations were performed primarily (94%) on Siemens MR imaging scanners and the remaining on GE Healthcare scanners. Scanner details are provided in the Online Supplemental Data. The protocol included sagittal T1, axial T2, precontrast axial T2 FLAIR, axial DTI, and postgadolinium (PG) 3D T1.

Volumetric analysis of the tumor was obtained by generating 3D ROIs on a Vitrea workstation (Canon Medical) using Vital 3D Medical Imaging software (Access Radiology) on the anatomic sequences. This procedure was performed on the T2 FLAIR imaging by delineating the abnormal T2-hyperintense signal seen in the pons. When T2 FLAIR was unavailable, this parameter was estimated using a 2D T2 TSE sequence. The volume of enhancing tumor was assessed on the PG 3D T1 sequence.

ADC maps from the DTI data were generated on the scanner in most cases and off-line using OsiriX (Pixmeo SARL) when scanner-generated ADC maps were not available. To generate the ADC histogram, we registered ADC maps to the anatomic sequence of interest (T2 FLAIR or T2 and PG T1) using tools from the FSL library (<http://www.fmrib.ox.ac.uk/fsl>),<sup>29</sup> previously described by Poussaint et al.<sup>17</sup> In summary,  $b = 0$  (and subsequently the ADC map) was transformed into the space of the anatomic sequences, and 3D ROIs were created using the thresholding feature in Fiji (<http://fiji.sc>),<sup>30</sup> an Open Source (<https://opensource.org/>) distribution of Java modules along with ImageJ software (National Institutes of Health). Values from every pixel in the tumor volume from the ADC map were then extracted, and histograms were generated. Within each tumor, values of the mean, SD, median, mode, skewness, and kurtosis of the ADC histogram for the total tumor volume (referred to as ADC<sub>total</sub>) and the enhancing tumor volume (referred to as ADC<sub>enhancement</sub>) were used for statistical analysis. The choice of these ADC histogram metrics was based on previous studies.<sup>14,19</sup>

### Statistical Analysis

Clinical and demographic variables were summarized using descriptive statistics. Continuous measures were summarized using medians and ranges. Categorical measures were summarized using frequencies and proportions. Kaplan-Meier curves of OS were generated, and point estimates of OS  $\pm$  standard error were presented at 6, 12, and 18 months. The histone H3 mutation groups were tested for association with OS using a log-rank test. Continuous variables (mean ADC<sub>total</sub>, median ADC<sub>total</sub>, mode of ADC<sub>total</sub>, mean ADC<sub>enhancement</sub>, and median ADC<sub>enhancement</sub>) were dichotomized on the median value and tested for association with OS using a log-rank test. The Wilcoxon rank-sum test was used to compare continuous imaging predictors between categorical end points of the histone mutation groups. The Fisher exact test was used to compare categorical imaging predictors (presence/absence of tumor volume enhancement versus molecular subgroup). Two-sided *P* values  $\leq .05$  were considered statistically significant. Given the hypothesis-generating nature of these analyses, no adjustment for multiple hypothesis testing was performed. R statistical and computing

**Table 1: Baseline characteristics of patients with pontine pHGG (n = 83)**

Patient Characteristic	No. (%) or Median (Range)
Sex	
Male	43 (52)
Female	40 (48)
Race	
White	60 (72)
Black	19 (23)
Other	4 (5)
Age at registration (yr)	6 (0.7–17)
Histone mutation status	
H3-3A	50 (60)
H3C2/3	11 (13)
Wild-type	15 (18)
H3 K27–altered, specific gene unknown	7 (8)
Presence of enhancement	
Yes	54
No	25
Unknown	4
Median follow-up time of surviving patients (mo)	10.3 (2.3–76.2)

software Version 3.5.0 (<http://www.r-project.org>) and SAS Version 9.4 (SAS Institute) were used for statistical analyses.

## RESULTS

### Patient Population Characteristics

There were 305 consecutively treated children with suspected pontine pHGG. Eighty-three patients met the eligibility criteria with MR imaging features of pontine pHGG on pretreatment MR imaging and evaluable tissue sampling. Of the 83 patients in the study, biopsy samples were obtained from 26 patients, and postmortem material, from 50 patients for genetic testing. Of these, 73 patients had evaluable DTI data at baseline (Online Supplemental Data) and were included for all ADC histogram analyses. In addition, 29 of 73 patients were treated during the study time period (September 2002 to December 2009).

The median age and follow-up time were 6 years (range, 0.7–17 years) and 10.3 months (range, 2.3–76.2 months), respectively.

The cohort consisted of 43 (52%) male and 40 (48%) female patients, of whom 23 (28%) were nonwhite. H3 K27–altered tumors were categorized as follows in Table 1: H3-3A ( $n = 50$ ; 60%), H3C2/3 ( $n = 11$ ; 13%), H3-mutant specific gene unknown ( $n = 7$ ; 8%), and wild-type ( $n = 15$ ; 18%).

### Histone Mutation, Overall Survival, and ADC Histogram Metrics

The mean OS at 12 months for all patients was 37% [SD, 5.5%] (Online Supplemental Data).

Children with H3C2/3-mutant tumors ( $n = 11$ ) had significantly higher OS compared with those with H3-3A mutation ( $n = 50$ ) (73% [SD, 13.4%] versus 17 [SD, 5.6%] at 1 year, respectively;  $P = .003$ ) (Online Supplemental Data and Fig 1A). Those patients with H3 wild-type HGG tumors ( $n = 15$ ) had significantly higher OS compared with H3C2/3- and H3-3A-mutant tumors (63% [SD, 13.3%] versus 32% [SD, 5.8%] at 1 year, respectively;  $P = .001$ ) (Online Supplemental Data and Fig 1B).

The OS was significantly lower in patients with enhancing tumors compared with patients whose tumors showed no enhancement (29% [SD, 6.5%] versus 56% [SD, 10%] at 1 year, respectively;  $P = .02$ ) (Online Supplemental Data).

However, there was no statistical association between histone H3 mutation groups and the presence of enhancement:  $P = .2$  for the association of enhancement and histone mutations (H3-3A versus H3C2/3) and  $P = .7$  for the association of enhancement with any histone mutation versus wild-type.

When we compared group median values, the H3-3A-mutant group ( $n = 46$ ) demonstrated lower values of mean ADC<sub>total</sub> ( $P < .001$ ), median ADC<sub>total</sub> ( $P < .001$ ), mode ADC<sub>total</sub> ( $P < .001$ ), mean (PG) ADC<sub>enhancement</sub> ( $P = .004$ ), median (PG) ADC<sub>enhancement</sub> ( $P = .003$ ), and mode (PG) ADC<sub>enhancement</sub> ( $P = .002$ ) compared with the H3C2/3-mutant group ( $n = 9$ ) (Table 2 and Fig 2A). Skewness ADC<sub>total</sub> ( $P = .003$ ) and kurtosis ADC<sub>total</sub> ( $P = .002$ ) were significantly higher in H3-3A- versus H3C2/3-mutant tumors (Table 2 and Fig 2B).

There was no significant difference in ADC histogram metrics between H3 wild-type ( $n = 12$ ) and mutant tumors ( $n = 61$ ), even though the survival of patients with wild-type tumors was significantly longer (Table 3).

### Histone Mutation and Tumor Volume

The total tumor volume varied among mutation groups; however, these differences did not meet statistical significance ( $P = .2$  and 0.8, respectively) (Tables 2 and 3). No significant differences in the volume of tumor enhancement were identified between the various mutational profiles (H3-3A versus H3C2/3 ( $P = .6$ ) and any histone H3 mutation versus wild-type ( $P = .4$ ) (Tables 2 and 3).

## DISCUSSION

Advances in genomic and epigenetic analyses have led to an improved understanding of the clinical and biologic behavior of pontine HGGs.<sup>13</sup> The discovery of histone H3 mutations in 70%–84% of pontine pHGGs was an important turning point in our understanding of this tumor.<sup>10,31–33</sup> Clinoradiologic and prognostic criteria were then refined with histone H3 genotyping because mutations in the H3-3A- and H3C2/3 genes correlate with different phenotypical and biologic behaviors and differences in OS.<sup>20,25</sup> Prior work by Jaimes et al<sup>24</sup> demonstrated differences in ADC histogram parameters and enhancement among various histone mutations of pontine HGG. This radiogenomic tool offers a framework for differentiating these alterations non-invasively and, most important, identifying those that have a worse overall survival. In this study, we examined whether radiomics could distinguish among molecular subtypes of pontine pHGG with similar/overlapping phenotypes on conventional anatomic MR images and with ADC histogram parameters.<sup>17,18,24</sup> ADC values in this study were all derived from DTI data rather than routine clinical DWIs.

Correlations among ADC values, tumor cellularity, and response to treatment in low-grade and high-grade pediatric brain tumors have been previously studied.<sup>34–36</sup> The ADC histogram is a valuable tool for describing diffusion characteristics in the total tumor volume on T2 FLAIR and postcontrast T1-weighted images.

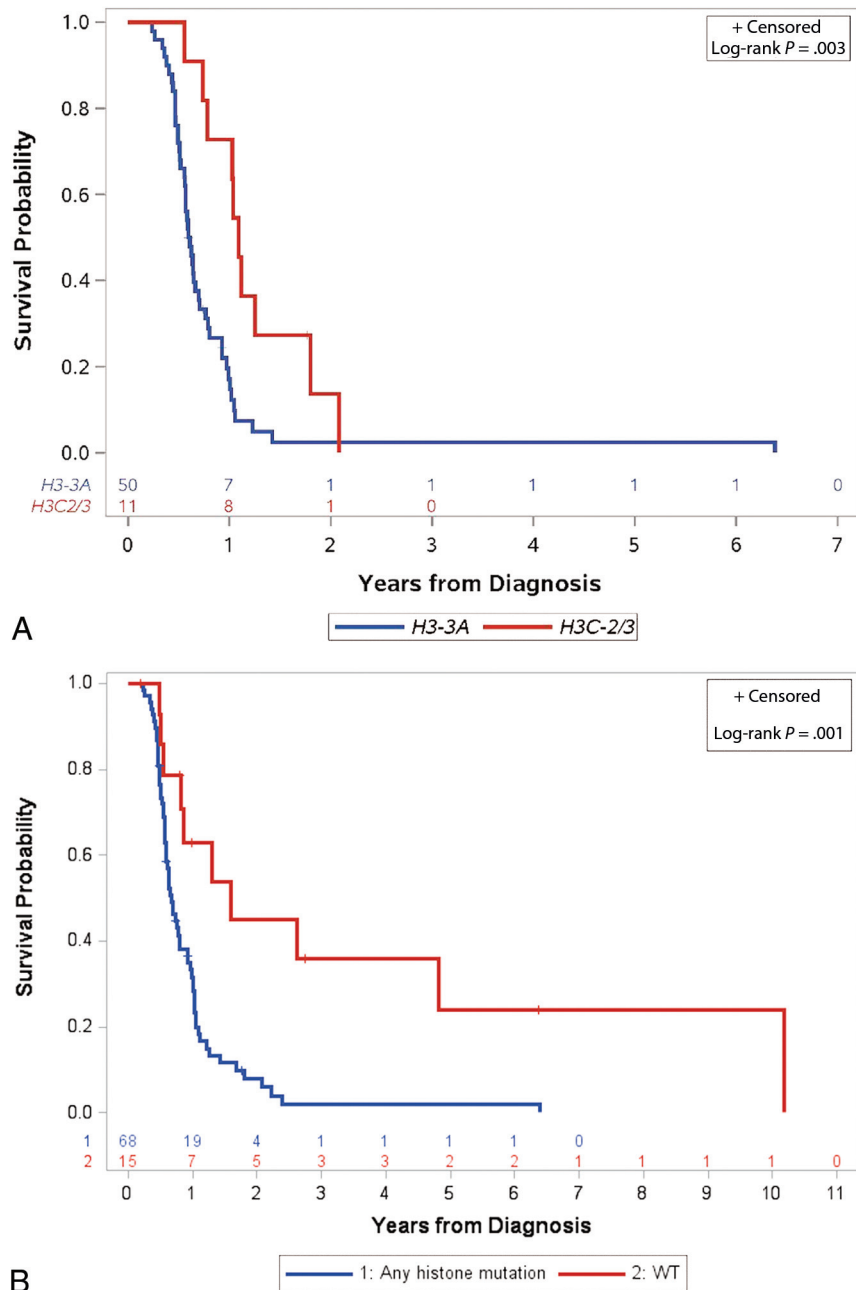


**FIG 1.** Differences in OS between variant histone profiles. **A**, Kaplan-Meier curves of a patient's OS by histone H3 mutation: *H3-3A* ( $n = 50$ ) versus *H3C2/3* ( $n = 11$ ). **B**, Kaplan-Meier curves of OS for patients with tumors with histone H3 mutation (*H3-3A*, *H3C2/3*, and H3-mutant, specific gene unknown) ( $n = 68$ ) versus H3 wild-type ( $n = 15$ ) tumors.

Key ADC histogram metrics found to correlate with survival, treatment response, and mutational status are the mean, SD, median, mode, skewness, and kurtosis of the ADC histogram for the total tumor volume and the enhancing tumor volume.<sup>17,24</sup> This study focuses on those ADC metrics in our statistical analyses to limit the number of comparisons, thereby increasing statistical power. Poussaint et al<sup>17</sup> previously studied the correlation between ADC histogram metrics and progression-free survival in patients with pontine HGGs. Although tumor molecular characteristics were not studied in the aforementioned work, the authors found 2 peak histogram distributions (unimodal and bimodal), with the unimodal peak increased skewness likely due to increasing cellularity.

Poussaint et al also reported that the mean ADC was lower in children with shorter survival. Chen et al<sup>37</sup> found a negative correlation between fractional anisotropy and survival, and although the correlation between ADC histograms and tumor profiles was not studied, one may extrapolate that lower ADC values correlated with more aggressive tumor behavior.

Castel et al<sup>20</sup> reported that MR imaging features correlated histologically with extensive extracellular edema, present primarily within *H3C2/3*- compared with *H3-3A*-mutant tumors. ADC values were lower in *H3-3A*-mutant tumors, concurring with this work. This may be attributed to the differences in the oncogenic mechanisms of these alterations. Jaimes et al<sup>24</sup> suggested that



**Table 2: Association of measures of continuous imaging features with variant histone H3–altered tumors**

Imaging Metric	H3-3A		H3C2/3		P Value <sup>a</sup>
	No.	Median (Range)	No.	Median (Range)	
ADC total ( $\times 10^{-6}$ mm <sup>2</sup> /s)					
Mean	46	1227.51 (538.06–1710.88)	9	1586.56 (1224.37–1797.58)	.001
Median	46	1185 (532–1755)	9	1654 (1215–1842)	.001
Mode	46	1168.14 (450.92–1902.53)	9	1703.88 (1263.52–1961.24)	.001
Skewness	38	0.91 (–0.49–2.16)	9	–0.20 (–0.89–0.88)	.003
Kurtosis	38	1.57 (–0.60–9.71)	9	0.40 (–0.78–1.79)	.002
ADC_enhancement ( $\times 10^{-6}$ mm <sup>2</sup> /s)					
Mean	33	1138.81 (689.44–1509.96)	7	1390.54 (1033.58–1898.26)	.004
Median	33	1085 (667–1532)	7	1364 (995–1890)	.003
Mode	33	1012.56 (577.86–1617.56)	7	1393.38 (966.31–1746.86)	.002
Skewness	31	1.27 (–0.56–2.82)	7	0.52 (–0.71–2.61)	.1
Kurtosis	31	2.08 (–0.94–13.03)	7	0.85 (–0.84–9.09)	.3
FLAIR/T2/T1 PG volume ( $\times 10^3$ mm <sup>3</sup> )					
FLAIR/T2	44	35.75 (7.97–77.53)	10	41.10 (22.84–77.57)	.2
Enhancing	32	1.90 (0.07–14.10)	9	5.04 (0.04–8.25)	.6

<sup>a</sup> Wilcoxon rank-sum test.

increased cellularity was the reason for the increased kurtosis and skewness in *H3-3A*-mutant tumors compared with *H3C2/3*-mutant tumors.

Calmon et al<sup>12</sup> also reported that *H3C2/3*-mutant tumors had higher ADC values than *H3-3A*-mutant tumors in 27 patients who underwent pretreatment MR imaging and biopsy for their pontine pHGGs. They also hypothesized that *H3C2/3*-mutant tumors demonstrated increased extracellular edema due to ion channel gene downregulation.<sup>12</sup> A higher positive nuclear density was noted relative to *H3C2/3*-mutant tumors, which they postulated may be secondary to interstitial edema differences. However, they did not perform quantitative analysis of the edema, and their study focused on only the biopsied sample of the tumor and not the total tumor volume. Furthermore, the *H3C2/3*- and *H3-3A*-mutant tumors showed associated histologic differences, with the former containing mesenchymal glioblastoma subtypes and astroglial cells and the latter containing proneural glioblastoma multiforme and oligodendrocytic signatures.<sup>20</sup>

Our analysis of ADC histogram metrics in *H3-3A*-mutant pontine pHGGs demonstrates significantly lower mean and median ADC values of total tumor volume with higher skewness and kurtosis than the *H3C2/3*-mutant tumors, concurring with the findings of Jaimes et al.<sup>24</sup> Our study reports no significant difference between ADC histogram metrics of wild-type and H3 K27–mutant profiles, consistent with the study published by Jaimes et al and Castel et al.<sup>38</sup> This result is likely related to the similar biologic phenotype of these 2 profiles with the loss of H3 K27 trimethylation. In addition, the heterogeneous nature of these tumors may also be a valid contributor. Pertinent to this study, Aboian et al<sup>18,26</sup> previously found no statistically significant association between the MR imaging characteristics of pontine wild-type or H3 K27–altered HGGs, specifically edema, enhancement, necrosis, and the infiltrative nature of the tumors.

Piccardo et al<sup>22</sup> found a statistical correlation between MR imaging parameters such as DWI, spectroscopy, and perfusion in pontine HGGs. Significantly lower ROI ADC values were found in H3 K27–altered tumors compared with H3 wild-type.

Their sample size was small and included HGGs in all locations, not just the pons. Furthermore, all the H3 K27–altered tumors included in their 22-patient cohort were *H3-3A*-mutant.

As mentioned previously and similar to the results published by Khuong-Quang et al,<sup>32</sup> we found that children with H3 wild-type HGGs have significantly higher OS compared with those with *H3-3A*- and *H3C2/3*-mutant tumors. We also found that children with *H3C2/3*-mutant tumors had significantly higher OS than those with an *H3-3A* mutation. This finding is concordant with the work of Castel et al,<sup>20</sup> which demonstrated that OS differs significantly between histone H3 alterations. *H3C2/3*-mutant tumors have an overall better prognosis because they tend to metastasize less frequently and may respond better to radiation therapy.

Similar results were reported in the studies by Calmon et al<sup>12</sup> and Jaimes et al,<sup>24</sup> who studied 27 and 50 patients with DIPGs, respectively. Additionally, patients with *H3C2/3*-mutant tumors tended to present at a younger age, approximately 2 years younger than patients with *H3-3A*-mutant tumors.<sup>12</sup>

In our cohort, enhancement was associated with a significantly worse OS, confirming previous studies.<sup>17,24</sup> However, the total tumor volume seen on T2 FLAIR or volume of enhancement was not significantly associated with OS. Similar to findings of Jaimes et al<sup>24</sup> and Calmon et al,<sup>12</sup> differences in enhancing volumes were higher, though not significantly, in *H3C2/3*- compared with *H3-3A*-mutant tumors, with the latter carrying a worse prognosis. This finding is likely multifactorial and may be explained by higher microvascular density and perhaps increased vascular/contrast leakage in *H3C2/3*, though also not statistically significant, and may not adequately reflect the internal milieu in these tumors.<sup>12</sup>

Our study has several limitations. All of the tumors in our cohort are pontine pHGGs, and future work will have to include HGGs in other locations. While our sample size is the largest to date to study associations of ADC histogram metrics with histone H3 gene alterations in pontine HGGs, these results should be validated in larger, prospective studies, given the breakdown in histone-altered tumor subsets. Second, we

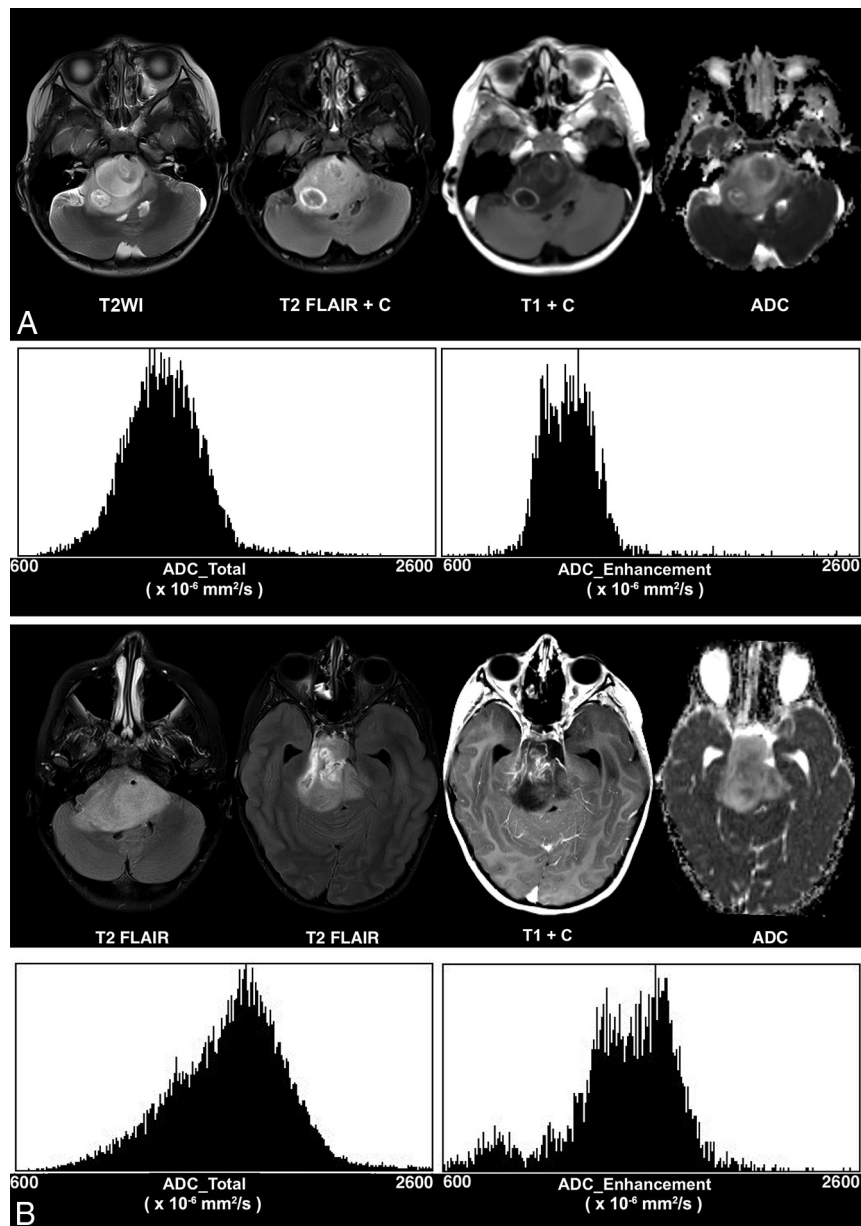


**FIG 2.** Differences in ADC histogram parameters among histone H3 K27-altered tumors. *H3-3A*-mutant tumor (A) shows lower ADC\_total mode ( $1252.531 \times 10^{-6} \text{ mm}^2/\text{s}$ ), higher ADC\_total skewness (0.673), and higher ADC\_total kurtosis (2.721) relative to *H3C2/3*-altered tumor (B) (ADC\_total mode:  $1703.875 \times 10^{-6} \text{ mm}^2/\text{s}$ ; ADC\_total skewness:  $-0.231$ ; and ADC\_total kurtosis: 0.399). *H3-3A*-mutated tumor (A) shows lower mean (PG) ADC\_enhancement ( $1216.092 \times 10^{-6} \text{ mm}^2/\text{s}$ ), median (PG) ADC\_enhancement ( $1206 \times 10^{-6} \text{ mm}^2/\text{s}$ ), and mode (PG) ADC\_enhancement ( $1103.723 \times 10^{-6} \text{ mm}^2/\text{s}$ ), relative to *H3C2/3*-mutated tumor (B): mean (PG) ADC\_enhancement ( $1461.677 \times 10^{-6} \text{ mm}^2/\text{s}$ ), median (PG) ADC\_enhancement ( $1500 \times 10^{-6} \text{ mm}^2/\text{s}$ ), and mode (PG) ADC\_enhancement ( $1665.322 \times 10^{-6} \text{ mm}^2/\text{s}$ ). A, A 3-year-old girl with *H3-3A*-mutant diffuse midline glioma and OS = 217 days. B, An 8-year-old girl with *H3C2/3*-mutant diffuse midline glioma and OS = 761 days.

did not perform a direct correlation to the histologic data or include advanced imaging techniques such as perfusion in our multiparametric MR imaging analysis. Third, we did not test for *EZH1P* overexpression and *IDH1/2* mutations in our tumor samples and did not perform DNA methylation profiling for tumor subtyping; therefore, we cannot distinguish different tumor subtypes in our H3 wild-type category. Finally, the studies in this retrospective analysis were performed during 18 years and on multiple scanners at the same institution. ADC values have been found to be fairly consistent across scanner types and strengths in both in vivo<sup>39</sup> and in phantom studies,<sup>40</sup> and the

ADC values found in this study are consistent with those in the literature.<sup>17,24</sup> However, the possible variability of ADC values derived from DTI data from multiple scanners may still be a limitation of this study.

Future work may incorporate machine learning algorithms on large data sets to expand our knowledge of the biologic features of these tumors. Wagner et al<sup>41</sup> found radiomics features on standard MR imaging that were associated with progression-free survival in pediatric diffuse pontine glioma not based on mutational status. Future applications could incorporate mutational analyses in a larger data set.

**Table 3: Association of measures of continuous imaging features with variant histone H3–altered versus H3 wild-type tumors**

Imaging Metric	Any Histone Mutation		Wild-Type		P Value <sup>a</sup>
	No.	Median (Range)	No.	Median (Range)	
ADC total ( $\times 10^{-6}$ mm <sup>2</sup> /s)					
Mean	61	1302.42 (538.06–1797.58)	12	1350.77 (922.96–1729.62)	.98
Median	61	1245 (532–1842)	12	1345 (917–1781)	.97
Mode	61	1250.51 (450.92–1961.24)	12	1305.29 (863.39–1805.47)	.9
Skewness	52	0.68 (–0.89–3.11)	11	0.98 (–0.30–2.57)	.3
Kurtosis	52	1.4 (–0.78–15.62)	11	2.82 (–0.78–10.77)	.1
ADC_enhancement ( $\times 10^{-6}$ mm <sup>2</sup> /s)					
Mean	45	1152.88 (689.44–1898.26)	6	1199.86 (956.62–1723.18)	.7
Median	45	1142.00 (667–1890)	6	1187.00 (807–1762)	.7
Mode	45	1062.49 (577.86–1746.86)	6	1175.10 (719.70–1805.78)	.6
Skewness	43	0.86 (–0.85–4.73)	6	0.67 (–0.14–1.86)	.7
Kurtosis	43	1.69 (–0.94–29.06)	6	1.35 (0.098–12.45)	.9
FLAIR/T2/T1 PG volume ( $\times 10^3$ mm <sup>3</sup> )					
FLAIR/T2	60	35.13 (7.97–77.57)	13	32.77 (10.13–79.62)	.8
Enhancing	46	1.96 (0.04–14.10)	8	1.95 (0.01–4.71)	.4

<sup>a</sup> Wilcoxon rank-sum test.

## CONCLUSIONS

MR imaging features, including ADC histogram metrics, are different across *H3C2/3*-, *H3-3A*-mutant, and H3 wild-type pontine HGGs. Future advances in noninvasive imaging approaches will seek to improve our understanding of the biology and physiology of these aggressive tumors and will help prognosticate survival.

## ACKNOWLEDGMENTS

This work is in memory of our wonderful friend and colleague Zoltan Patay, MD, PhD, who contributed to this work and was dedicated to improving the health of children everywhere.

Disclosure forms provided by the authors are available with the full text and PDF of this article at [www.ajnr.org](http://www.ajnr.org).

## REFERENCES

- Barkovich AJ, Krischer J, Kun LE, et al. Brain stem gliomas: a classification system based on magnetic resonance imaging. *Pediatr Neurosurg* 1990;16:73–83 [CrossRef Medline](#)
- Louis DN, Perry A, Reifenberger G, et al. The 2016 World Health Organization Classification of Tumors of the Central Nervous System: a summary. *Acta Neuropathol* 2016;131:803–20 [CrossRef Medline](#)
- Louis DN, Perry A, Wesseling P, et al. The 2021 WHO Classification of Tumors of the Central Nervous System: a summary. *Neuro Oncol* 2021;23:1231–51 [CrossRef Medline](#)
- Varlet P, Baker SJ, Ellison DW, et al. Diffuse midline glioma, H3 K27-altered. In: WHO Classification of tumors editorial boards. *WHO Classification of Tumours: Central Nervous System Tumours*. 5th ed. IARC Press; 2021:69–73
- Hoffman LM, Veldhuijzen van Zanten SE, Colditz N, et al. Clinical, radiologic, pathologic, and molecular characteristics of long-term survivors of diffuse intrinsic pontine glioma (DIPG): a collaborative report from the International and European Society for Pediatric Oncology DIPG Registries. *J Clin Oncol* 2018;36:1963–72 [CrossRef Medline](#)
- Ostrom QT, Patil N, Cioffi G, et al. CBTRUS Statistical Report: Primary Brain and Other Central Nervous System Tumors Diagnosed in the United States in 2013–2017. *Neuro Oncol* 2020;22:iv1–96 [CrossRef Medline](#)
- Leach JL, Roebker J, Schafer A, et al. MR imaging features of diffuse intrinsic pontine glioma and relationship to overall survival: report from the International DIPG Registry. *Neuro Oncol* 2020;22:1647–57 [CrossRef Medline](#)
- Albright AL, Packer RJ, Zimmerman R, et al. Magnetic resonance scans should replace biopsies for the diagnosis of diffuse brain stem gliomas: a report from the Children's Cancer Group. *Neurosurgery* 1993;33:1026–29; discussion 1029–30 [CrossRef Medline](#)
- Puget S, Beccaria K, Blauwblomme T, et al. Biopsy in a series of 130 pediatric diffuse intrinsic pontine gliomas. *Childs Nerv Syst* 2015;31:1773–80 [CrossRef Medline](#)
- Wu G, Diaz AK, Paugh BS, et al. The genomic landscape of diffuse intrinsic pontine glioma and pediatric non-brainstem high-grade glioma. *Nat Genet* 2014;46:444–50 [CrossRef Medline](#)
- Gupta N, Goumnerova LC, Manley P, et al. Prospective feasibility and safety assessment of surgical biopsy for patients with newly diagnosed diffuse intrinsic pontine glioma. *Neuro Oncol* 2018;20:1547–55 [CrossRef Medline](#)
- Calmon R, Dangouloff-Ros V, Varlet P, et al. Radiogenomics of diffuse intrinsic pontine gliomas (DIPGs): correlation of histological and biological characteristics with multimodal MRI features. *Eur Radiol* 2021;31:8913–24 [CrossRef Medline](#)
- Mackay A, Burford A, Carvalho D, et al. Integrated molecular meta-analysis of 1,000 pediatric high-grade and diffuse intrinsic pontine glioma. *Cancer Cell* 2017;32:520–537.e5 [CrossRef Medline](#)
- Kfoury-Beaumont N, Prakasam R, Pondugula S, et al. The H3K27M mutation alters stem cell growth, epigenetic regulation, and differentiation potential. *BMC Biol* 2022;20:124 [CrossRef Medline](#)
- Lu VM, Power EA, Zhang L, et al. Liquid biopsy for diffuse intrinsic pontine glioma: an update. *J Neurosurg Pediatr* 2019 Sep 6. [Epub ahead of print] [CrossRef Medline](#)
- Azad TD, Jin MC, Bernhardt LJ, et al. Liquid biopsy for pediatric diffuse midline glioma: a review of circulating tumor DNA and cerebrospinal fluid tumor DNA. *Neurosurg Focus* 2020;48:E9 [CrossRef Medline](#)
- Poussaint TY, Vajapeyam S, Ricci KI, et al. Apparent diffusion coefficient histogram metrics correlate with survival in diffuse intrinsic pontine glioma: a report from the Pediatric Brain Tumor Consortium. *Neuro Oncol* 2016;18:725–34 [CrossRef Medline](#)
- Aboian MS, Tong E, Solomon DA, et al. Diffusion characteristics of pediatric diffuse midline gliomas with histone H3-K27M mutation using apparent diffusion coefficient histogram analysis. *AJNR Am J Neuroradiol* 2019;40:1804–10 [CrossRef Medline](#)
- Zhang P, Duan Y, Gu G, et al. Clinical, pathological, and radiological features of 80 pediatric diffuse intrinsic pontine gliomas: a single-institute study. *Front Oncol* 2023;13:1007393 [CrossRef Medline](#)
- Castel D, Philippe C, Calmon R, et al. Histone H3F3A and HIST1H3B K27M mutations define two subgroups of diffuse intrinsic pontine



- gliomas with different prognosis and phenotypes. *Acta Neuropathol* 2015;130:815–27 [CrossRef Medline](#)
21. Castel D, Grill J, Debily MA. Histone H3 genotyping refines clinicoradiological diagnostic and prognostic criteria in DIPG. *Acta Neuropathol* 2016;131:795–96 [CrossRef Medline](#)
  22. Piccardo A, Tortora D, Mascelli S, et al. Advanced MR imaging and <sup>18</sup>F-DOPA PET characteristics of H3K27M-mutant and wild-type pediatric diffuse midline gliomas. *Eur J Nucl Med Mol Imaging* 2019;46:1685–94 [CrossRef Medline](#)
  23. Lapin DH, Tsoli M, Ziegler DS. Genomic insights into diffuse intrinsic pontine glioma. *Front Oncol* 2017;7:57 [CrossRef Medline](#)
  24. Jaimes C, Vajapeyam S, Brown D, et al. MR imaging correlates for molecular and mutational analyses in children with diffuse intrinsic pontine glioma. *AJNR Am J Neuroradiol* 2020;41:874–81 [CrossRef Medline](#)
  25. Giagnacovo M, Antonelli M, Biassoni V, et al. Retrospective analysis on the consistency of MRI features with histological and molecular markers in diffuse intrinsic pontine glioma (DIPG). *Childs Nerv Syst* 2020;36:697–704 [CrossRef Medline](#)
  26. Aboian MS, Solomon DA, Felton E, et al. Imaging characteristics of pediatric diffuse midline gliomas with histone H3 K27M mutation. *AJNR Am J Neuroradiol* 2017;38:795–800 [CrossRef Medline](#)
  27. Khalid F, Goya-Outi J, Escobar T, et al. Multimodal MRI radiomic models to predict genomic mutations in diffuse intrinsic pontine glioma with missing imaging modalities. *Front Med (Lausanne)* 2023;10:1071447 [CrossRef Medline](#)
  28. Chiang J, Diaz AK, Makepeace L, et al. Clinical, imaging, and molecular analysis of pediatric pontine tumors lacking characteristic imaging features of DIPG. *Acta Neuropathol Commun* 2020;8:57 [CrossRef Medline](#)
  29. Jenkinson M, Beckmann CF, Behrens TE, et al. FSL. *Neuroimage* 2012;62:782–90 [CrossRef Medline](#)
  30. Schindelin J, Arganda-Carreras I, Frise E, et al. Fiji: an open-source platform for biological-image analysis. *Nat Methods* 2012;9:676–82 [CrossRef Medline](#)
  31. Buczkowicz P, Hawkins C. Pathology, molecular genetics, and epigenetics of diffuse intrinsic pontine glioma. *Front Oncol* 2015;5:147 [CrossRef Medline](#)
  32. Khuong-Quang DA, Buczkowicz P, Rakopoulos P, et al. K27M mutation in histone H3.3 defines clinically and biologically distinct subgroups of pediatric diffuse intrinsic pontine gliomas. *Acta Neuropathol* 2012;124:439–47 [CrossRef Medline](#)
  33. Wu G, Broniscer A, McEachron TA, et al; St. Jude Children's Research Hospital–Washington University Pediatric Cancer Genome Project. Somatic histone H3 alterations in pediatric diffuse intrinsic pontine gliomas and non-brainstem glioblastomas. *Nat Genet* 2012;44:251–53 [CrossRef Medline](#)
  34. Koral K, Mathis D, Gimi B, et al. Common pediatric cerebellar tumors: correlation between cell densities and apparent diffusion coefficient metrics. *Radiology* 2013;268:532–37 [CrossRef Medline](#)
  35. Gauvain KM, McKinstry RC, Mukherjee P, et al. Evaluating pediatric brain tumor cellularity with diffusion-tensor imaging. *AJR Am J Roentgenol* 2001;177:449–54 [CrossRef Medline](#)
  36. Chenevert TL, Ross BD. Diffusion imaging for therapy response assessment of brain tumor. *Neuroimaging Clin N Am* 2009;19:559–71 [CrossRef Medline](#)
  37. Chen HJ, Panigrahy A, Dhall G, et al. Apparent diffusion and fractional anisotropy of diffuse intrinsic brain stem gliomas. *AJNR Am J Neuroradiol* 2010;31:1879–85 [CrossRef Medline](#)
  38. Castel D, Kergrohen T, Tauziède-Espariat A, et al. Histone H3 wild-type DIPG/DMG overexpressing EZHIP extend the spectrum diffuse midline gliomas with PRC2 inhibition beyond H3-K27M mutation. *Acta Neuropathol* 2020;139:1109–13 [CrossRef Medline](#)
  39. Merhem Z, Imsirovic B, Bilalovic N, et al. Apparent diffusion coefficient reproducibility in brain tumors measured on 1.5 and 3 T clinical scanners: a pilot study. *Eur J Radiol* 2018;108:249–53 [CrossRef Medline](#)
  40. Mulkern RV, Ricci KI, Vajapeyam S, et al. Pediatric brain tumor consortium multisite assessment of apparent diffusion coefficient z-axis variation assessed with an ice-water phantom. *Acad Radiol* 2015;22:363–69 [CrossRef Medline](#)
  41. Wagner MW, Namdar K, Napoleone M, et al. Radiomic features based on MRI predict progression-free survival in pediatric diffuse midline glioma/diffuse intrinsic pontine glioma. *Can Assoc Radiol J* 2023;74:119–26 [CrossRef Medline](#)